11. Bernstein, F. C. *et al*. The protein data bank: A computer-based archival file for macromolecular structures. *J. Biol. Chem.* **112,** 535–542 (1977).
12. Kitao, A., Hirata, F. & Go, N. The effects of solvent on the conformation and collective motions of protein: Normal mode analysis and molecular dynamics simulations of melittin in water and in vacuum. *Chem. Phys.* **158,** 447–472 (1991).
13. Mehrotra, P. K. & Beveridge, D. L. Structural analysis of molecular solutions based on quasi-component distribution functions. Application to $[H_2CO]_{aq}$ at 25 °C. *J. Am. Chem. Soc.* **102,** 4287–4294 (1980).
14. Zichi, D. A. & Rossky, P. J. The equilibrium solvation structure for the solvent-separated hydrophobic bond. *J. Chem. Phys.* **83,** 797–808 (1985).
15. Rossky, P. J. & Karplus, M. Solvation. A molecular dynamics study of a dipeptide in water. *J. Am. Chem. Soc.* **101,** 1913–1937 (1979).
16. Pascual-Ahuir, J. L., Silla, E. & Tunon, I. GEPOL: An improved description of molecular surfaces. III. A new algorithm for the computation of the solvent-excluding surface. *J. Comput. Chem.* **15,** 1127–1138 (1994).
17. Freire, E., Murphy, K. P., Sanchez-Ruiz, J. M., Galiseo, M. L. & Privalov, P. L. The molecular basis of cooperativity in protein folding. Thermodynamic dissection of interdomain interactions in phosphoglycerate kinase. *Biochemistry* **31,** 250–256 (1992).
18. Berendsen, H. J. C., Postma, J. P. M., van Gunsteren, W. F. & Hermans, J. in *Intermolecular Forces* (ed. Pullman, B.) 331–342 (Reidel, Dordrecht, 1981).
19. Jorgensen, W. L. & Tirado-Rives, J. The OPLS potential functions for proteins. Energy minimizations for crystals of cyclic peptides and crambin. *J. Am. Chem. Soc.* **110,** 1657–1671 (1988).
20. Verlet, L. Computer "experiments" on classical fluids. I. Thermodynamical properties of Lennard–Jones molecules. *Phys. Rev.* **159,** 98–103 (1967).
21. Ryckaert, J.-P., Ciccotti, G. & Berendsen, H. J. C. Numerical integration of the Cartesian equations of motion of a system with constraints: Molecular dynamics of *n*-alkanes. *J. Comput. Phys.* **23,** 327–341 (1977).
22. Nicholls, A., Sharp, K. A. & Honig, B. Protein folding and association: Insights from the interfacial and thermodynamic properties of hydrocarbons. *Proteins* **11,** 281–296 (1991).

Acknowledgements. We acknowledge contributions from W. S. Sheu and T. S. Cohen in the early stages of this work. This work was supported by the NIH.

Correspondence and requests for materials should be addressed to P.J.R. (e-mail: rossky@mail.utexas.edu).

Millennial-scale climate instability during the early Pleistocene epoch

M. E. Raymo*, K. Ganley*, S. Carter*, D. W. Oppo† & J. McManus†

* *Department of Earth, Atmospheric and Planetary Sciences, Massachusetts Institute of Technology, Cambridge, Massachusetts 02139, USA*
† *Department of Geology and Geophysics, Woods Hole Oceanographic Institution, Woods Hole, Massachusetts 02543, USA*

Climate-proxy records of the past 100,000 years show that the Earth's climate has varied significantly and continuously on timescales as short as a few thousand years (refs 1–7). Similar variability has also recently been observed for the interval 340–500 thousand years ago[8]. These dramatic climate shifts, expressed most strongly in the North Atlantic region, may be linked to—and possibly amplified by—alterations in the mode of ocean thermohaline circulation[4–9]. Here we use sediment records of past iceberg discharge and deep-water chemistry to show that such millennial-scale oscillations in climate occurred over one million years ago. This was a time of significantly different climate boundary conditions; not only was the early Pleistocene epoch generally warmer, but global climate variations were governed largely by changes in Earth's orbital obliguity. Our results suggest that such millennial-scale climate instability may be a pervasive and long-term characteristic of Earth's climate, rather than just a feature of the strong glacial–interglacial cycles of the past 800,000 years.

Much has been learned about natural climate variability through the study of ice and sediment cores. In Greenland ice cores, variations of 5–8 °C in mean annual air temperature, called Dansgaard–Oeschger cycles, occur with a rough 1–3 kyr spacing throughout the last glacial cycle[1]. Within deep-sea cores, we observe correlative variations in sea surface temperature (SST), iceberg discharge, and possibly thermohaline circulation[2–9]. The origin of these millennial-scale climate cycles is not well understood; they have been attributed to forcing mechanisms internal to the climate system, such as ice-sheet dynamics or ocean–atmosphere interactions[4,10,11], as well as to mechanisms external to the climate system, such as solar variability[12] or combination tones of the main Milankovitch cycles[13,14]. Here we examine the characteristics of climate variability within this frequency band under a markedly different climate regime when glacial episodes were less severe[15], atmospheric CO_2 concentrations may have been higher[15–17], and climate over much of the globe (including ice sheets) varied almost exclusively at the 41-kyr period of orbital obliquity[15,18–20].

To recover such old sediment, we used the unique deep recovery capabilities of the drilling vessel *JOIDES Resolution*. To obtain the required temporal resolution, we drilled the rapidly accumulating Gardar sediment drift located south of Iceland (Fig. 1). Sedimentation rates at this location are enhanced by the horizontal advection of fine (<63-μm) material suspended in a nepheloid layer associated with Norwegian Sea Overflow Water spilling over the Iceland–Faeroe–Scotland ridge[21]. Hence, these sediments record physical and chemical changes in the downwelling limb of the global thermohaline 'conveyer belt', changes which strongly influence the circum-Atlantic (and perhaps global) climate[2,4].

Ocean Drilling Program (ODP) Site 983, recovered at 1,983 m water depth, accumulated continuously throughout the Pleistocene at rates >13 cm kyr^{-1} (ref. 22). Oxygen isotope measurements on the benthic foraminifera genus *Cibicidoides* (primarily *C. wuellerstorfi*) were made every ~38 cm (or ~2,500 yr) for a 27-m section of core spanning the early Pleistocene (Fig. 2). The presence of the Jaramillo (top and bottom) and Cobb Mountain magnetic reversals, diagnostic biostratigraphic datums (including the last occurrence of *Gephyrocapsa* A-B; Fig. 2), and shipboard lithostratigraphic data[22] allowed us to correlate our record to a $\delta^{18}O$ reference curve from DSDP Site 607[15] (Fig. 2a). We were then able to assign marine isotope stage (MIS) designations[15,20] to the site 983 $\delta^{18}O$ record (Fig. 2b). Ages for the mid-points of oxygen isotope stages, derived from the astronomically tuned timescale of Shackleton *et al*.[23], are given

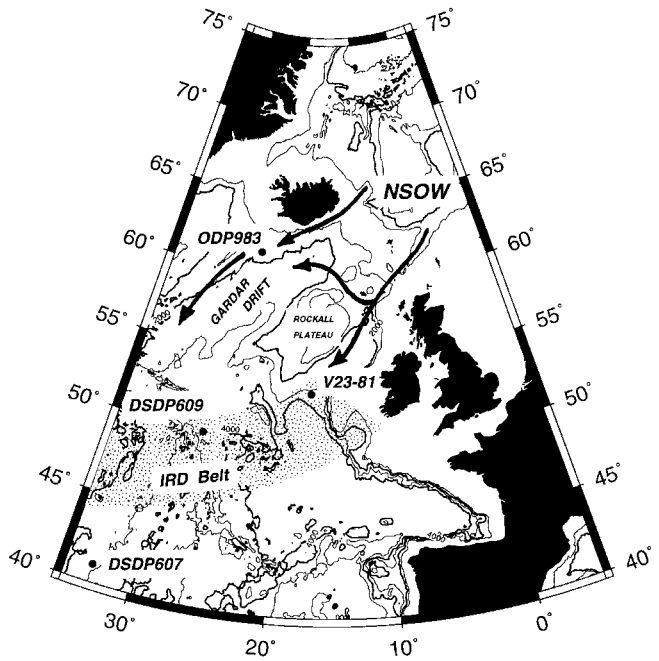

Figure 1 Location of study area. Map shows the location of core investigated in this study (ODP Site 983 at 60° 24′ N, 23° 38′ W and 1,983 m water depth) as well as DSDP sites 607 and 609, and V23-81 (ref. 3). Site 983 is located near the head of the Gardar drift which extends to the south-south-west, following the path of deep overflows (Norwegian Sea Overflow Water, NSOW, as shown by arrows) from the Iceland–Faeroe–Scotland ridge[21]. The location of the main ice-rafted debris (IRD) belt as determined for the last glacial cycle is shown by a stippled pattern.

in Fig. 3. Most of the $\delta^{18}O$ variance over this interval falls within the range of stage 5a–5d levels at this site[24].

To study the history of iceberg discharge to this region, the number of lithic fragments (>150 μm) per g of total sediment[3] was determined at orbital-scale resolution for the interval spanning MIS 36 to 45. Lithic grains >150 μm in size are delivered to the deep sea by the melting of drifting glacial ice[2,3,9,10] and the correlation of high values of lithic grains per g with positive $\delta^{18}O$ (Fig. 2b) reflects the expected relationship between periods of ice-sheet growth and iceberg discharge into the North Atlantic.

To examine suborbital variations in iceberg delivery to the subpolar North Atlantic, lithic counts were made at much higher resolution (~5 cm spacing or 380 yr) within MIS 40 and 44 (Fig. 3a and b). Oxygen- and carbon-isotope data were measured for every sample where enough *Cibicidoides* could be found (>15 μg of carbonate). The record has noticeably poorer temporal resolution in the early glacial intervals due to a paucity of benthic foraminiferal specimens at these times. During each of the climate cycles studied, we observe episodic increases in the delivery of lithic grains to the site with the final lithic peak within each cycle occurring near the mid-point of the deglacial interval as defined by the $\delta^{18}O$ record. Intervals between lithic peaks typically have <1 lithic grain per g of sediment (and many horizons have no lithic grains in the entire sample). Hence, unless one invokes unreasonably large sedimentation rate changes, the lithic data must be recording the episodic input of ice-rafted detritus (IRD) to this site.

In both MIS 40 and 44, iceberg delivery of lithic material appears to be more pronounced (both in the magnitude and frequency of ice-rafting events) early in the glacial interval, a time also characterized by relatively lower flux of planktonic foraminifera to the sediment (early glacial, EG, interval in Fig. 3). At least six distinct episodes of ice-rafting are observed within glacial stage 40 and five within MIS 44. Given that a complete climate cycle at these times is only ~41 kyr in duration[20,23], the ice-rafting episodes, by default, must be occurring more frequently than every 7 kyr (6 episodes × 7 kyr > 41 kyr). If one made the typical assumption of constant sedimentation rate between age control points, then the lithic cycles between 163 and 165 m in MIS 40, for instance, would be spaced approximately 2.0–2.5 kyr apart. Assuming a generous range of uncertainty in the sedimentation rates, constrained by the observed degree of symmetry in the glacial–interglacial cycles when plotted to depth (Fig. 2), we estimate these events occur with a periodicity of between 1 and 5 kyr during glacial intervals. Further improvement in chronostratigraphy may come from two sources: progress in understanding secular variations in the strength of the Earth's magnetic field and using these variations as a chronostratigraphic tool[24]; and second, examination of these (and other) specific intervals in different oceanographic settings so as to isolate regional climate versus local sedimentological effects.

Two other proxies for surface water hydrography were examined at this site: percentage *Neogloboquadrina pachyderma* sinistral (left-coiling), a planktonic foraminifera, and the shell $\delta^{18}O$ signature of *N. pachyderma* dextral (right-coiling). Both proxies have been shown to covary, during the last glacial cycle, with lithic fragment delivery especially within the main IRD belt[3,7]. However, in the early Pleistocene sections examined here, neither proxy shows a clear millennial-scale signal. This must partly be due to the extreme paucity of planktonic foraminifera within the early glacial interval of maximum lithic delivery (in one case 100% left-coiling *N. pachyderma* reflects the presence of only one planktonic specimen). Also, the location of the main IRD belt relative to Site 983 is unknown for the early Pleistocene, and it has been demonstrated that the surface water SST and meltwater signals are damped away from the main IRD belt (see, for example, ref. 7).

We also note that, in sediments of this age, evolutionary and environmental stability cannot be assumed for the *N. pachyderma* species (see, for example, refs 20, 25). Indeed, MIS 40 falls within an ~120-kyr-long interval of faunal assemblage variation which has no statistical, or analogous, counterpart in the late Pleistocene ocean[20,25]. This interval is characterized by the near complete absence of *N. pachyderma* sinistral from the North Atlantic, even during peak glacial periods characterized by the same benthic $\delta^{18}O$ and IRD signals as intervals (earlier and later) with abundant left-coiling *N. pachyderma*. (Similar anomalous patterns in the distribution of left-coiling *N. pachyderma* are observed before 1.7 Myr; ref. 20). Within the MIS 43–45 interval, *N. pachyderma* sinistral is present at 'normal' levels and reaches a maximum percentage abundance (if a very low absolute abundance) during the early glacial interval of maximum IRD delivery.

From the IRD data we conclude that millennial-scale variations in climate were occurring in the North Atlantic region over one million years ago. In addition, benthic $\delta^{18}O$ data, reflecting deep-water chemistry at 1,983 m water depth, present some of the clearest evidence yet found for a link, in the subpolar North Atlantic, between the periodic delivery of icebergs to the region and deep-water circulation changes which can transmit the effects of these regional climate changes around the globe. A number of the lithic peaks observed during MIS 44 and especially during MIS 40 are

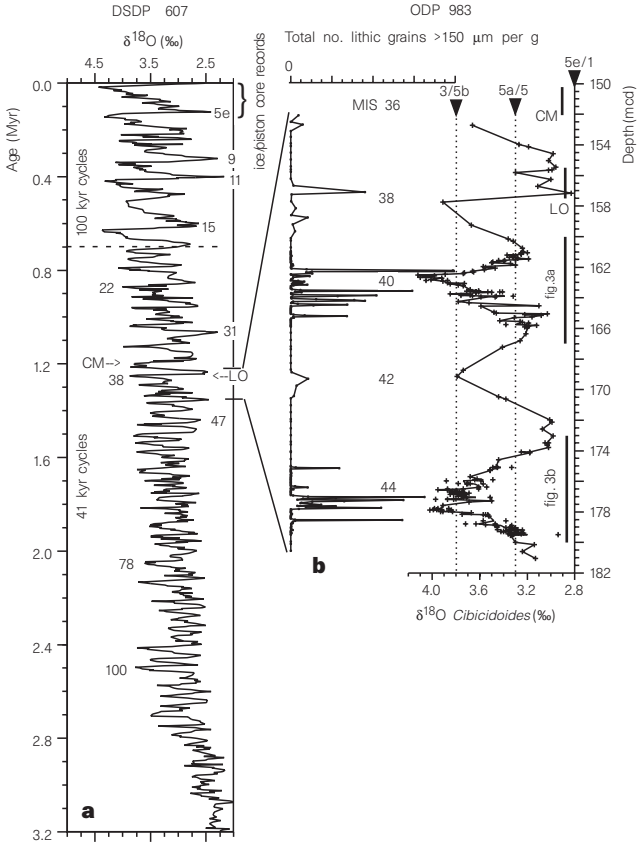

Figure 2 Data from deep-sea sediment cores. **a**, Variation in benthic $\delta^{18}O$ at DSDP Site 607 showing pattern of climate variation over past 3.2 Myr (ref. 15). CM indicates position of Cobb Mountain subchron identified in Site 607[20]; LO indicates position of *Gephyrocapsa* A-B datum[31]. Selected marine isotope stages (MIS) are labelled. **b**, 30-m section of early Pleistocene sediment examined from ODP Site 983, including total number of lithics per g of sediment (>15 μm) and $\delta^{18}O$ of benthic foraminifera *Cibicidoides*. The depth interval (in metres composite depth; ref. 22) of normal polarity representing the Cobb Mountain (CM) subchron is indicated by shaded bar to left of depth scale. The bar labelled LO indicates the depth range within which the last occurrence of the *Gephyrocapsa* spp. A-B datum occurs. Reference levels for typical $\delta^{18}O$ values during late Pleistocene interglacial stages at this site are shown on $\delta^{18}O$ curve. Note that 5b/5d levels are also approximately equivalent to high stage 3 levels. The higher density sampling within glacial stages 40 and 44 is shown at an expanded scale in Fig. 3.

associated with negative excursions in $\delta^{18}O$ of up to 0.4‰. As discussed below, these variations in deep-water chemistry do not originate in the surface waters over this site (hence, the fact that a strongly correlative isotopic signal is not observed in the planktonic $\delta^{18}O$ record is not unexpected.)

In attempting to explain the origin of these benthic $\delta^{18}O$ excursions, we note that a 0.4‰ decrease in $\delta^{18}O$ can be caused by a seawater warming of nearly 2 °C or by a decrease in salinity (or some combination of the two changes). If we assume that a salinity decrease is caused by the admixture of melt water and/or runoff to the water mass subducting north of our site (presumably the Norwegian–Greenland Sea), and also that this melt water has an isotopic value of −25‰, then subduction of only ~1.5% glacial melt water by volume would be needed to account for the magnitude of the observed $\delta^{18}O$ shifts. This amount of meltwater entrainment in the subducting surface water would cause a corresponding decrease in salinity of 0.5 and in density of ~0.4). How this less-dense water is then subducted to depth remains uncertain. Whereas Jansen and colleagues[26,27] suggest that brine formation under sea ice in the Norwegian–Greenland Sea is necessary to enhance surface water density to the degree that the meltwater signal can be convected to depth, the modelling results of Lehman *et al.*[28] suggest that the conveyor could entrain and advect a pulse of fresh water directly into the deep ocean.

An alternative hypothesis that has been proposed to explain similar depletions in $\delta^{18}O$ observed during the last glacial cycle is the replacement of deep water in this region by warmer Atlantic Intermediate Water[9]. Although speculative, we suggest that our benthic $\delta^{13}C$ data is most consistent with the hypothesis that a small amount of highly fractionated melt water is admixed into the subducting surface waters north of Site 983, and that this freshening causes the conveyor to weaken. In the modern ocean, a nearly constant $\delta^{13}C$ composition of ~1.1‰ characterizes water from 1,000 m to greater than 2,500 m depths at the location of Site 983 (ref. 29). During full glacial periods (for example, MIS 2 and 6), deep $\delta^{13}C$ values fall to ~0.5‰ at 2,500 m and increase to ~1.5‰ at 1,400 m, with the maximum gradient centred at the depth of Site 983 (ref. 29). The shallower nutrient-depleted water mass is Glacial North Atlantic Intermediate Water (GNAIW) while the deeper nutrient-enriched water mass originates from the Southern Ocean. If a light $\delta^{18}O$ excursion was indicative of the presence of warm GNAIW (see, for example, ref. 9) then a positive $\delta^{13}C$ shift would be expected. We observed the opposite trend, with $\delta^{13}C$ values typically decreasing over the course of an ice-rafting event and remaining low for approximately a millennium afterwards (the clearest expression of this lag is observed at ~163.6 and 163.9 m depth in the core).

Although such nutrient enrichment is consistent with the subduction of surface water originating in a region of greater than usual iceberg/sea-ice cover, we propose that during an ice-rafting episode, convection in the Norwegian–Greenland Sea begins to weaken owing to increasing melt water at the surface. Entrainment of a small amount of fresh water (<2%) weakens the overflows and limits the depth to which they can sink. This causes the boundary between water from the Southern Ocean and North Atlantic Deep Water to shoal, replacing northern source water with progressively more nutrient-enriched (low $\delta^{13}C$) southern source water. The unusually high $\delta^{13}C$ variability observed during glacial intervals strongly suggests that this site may have been situated near a water-mass boundary in the early Pleistocene as well as during the last glacial. Although this hypothesis is consistent with modelling results[28], further examination of this site in relation to deeper and shallower sites would be required to determine vertical nutrient distribution and hence the sources and structure of the glacial water masses.

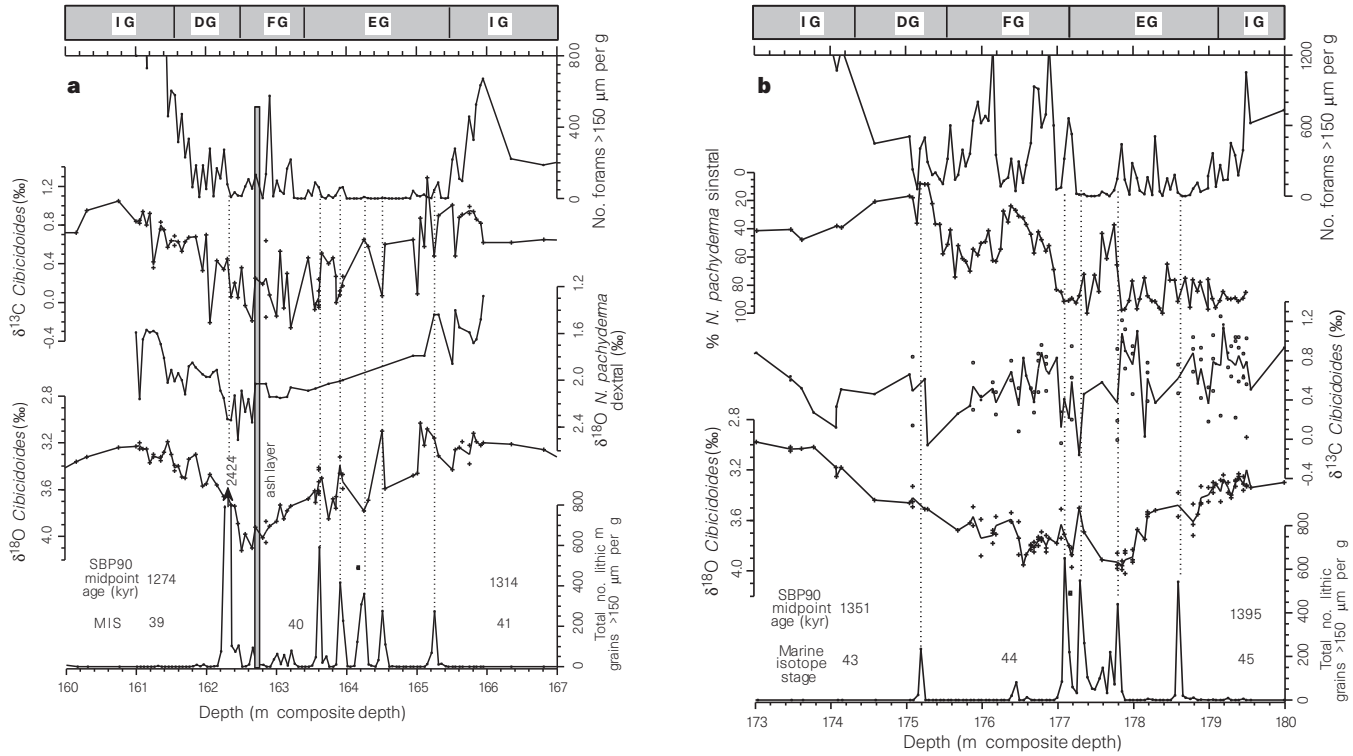

Figure 3 High-resolution isotopic, faunal and lithologic data from Site 983. **a**, MIS 39 to 41; **b**, MIS 43 to 45. Benthic isotopic measurements were based on *Cibicidoides*; planktonic isotopic and faunal measurements were on *N. pachyderma*. Ages given for the midpoints of warm stages are after the timescale of Shackleton *et al.* (SBP90)[23]. Vertical dashed lines delineate peaks in the delivery of ice-rafted material to this site. One sample horizon (983A-16-6, 94–98 cm with a lithics per g count of 8,400) was omitted from plot (and interval was labelled as 'ash layer') as it consisted almost entirely of frothy basaltic glass and probably represents an ash fall (a few non-basaltic lithic grains were observed in this sample, however, and the samples on either side were counted excluding frothy glass). Note also that almost all the benthic isotope analyses for MIS 44 were on single specimens resulting in more replicate analyses and greater variability in the $\delta^{13}C$ record, as would be expected from a site located near a strong $\delta^{13}C$ gradient. Abbreviations on top axes as follows: IG, interglacial; EG, early glacial; FG, full glacial; DG, deglacial.

We now consider why these rapid climate oscillations occurred in the first place; were they forced (or excited) by processes internal, or external, to the climate system? Here we have shown that millennial-scale variations in iceberg discharge were present over one million years ago and thus occur across a broader spectrum of climate boundary conditions than has been previously recognized. These variations, similar in character and timing to ice-rafting events associated with late Pleistocene Dansgaard–Oeschger cycles, occurred during a climate regime dominated by the obliquity component of orbital forcing and which was too warm to support the growth of large 100-kyr ice sheets[15,20,30]. Correlative variations in the chemical properties of deep North Atlantic water also suggest that glacial melt water associated with periodic ice-sheet mass wasting was entrained in Norwegian Sea Overflow Water, influencing the Atlantic thermohaline 'conveyor belt' and thus, potentially, global climate. □

Received 23 July 1997; accepted 17 February 1998.

1. Dansgaard, W. *et al.* in *Climate Processes and Climate Sensitivity* (eds Hansen, J. E. & Takahashi, T.) 288–298 (Am. Geophys. Union, Washington DC, 1984).
2. Broecker, W. S. Massive iceberg discharges as triggers for global climate change. *Nature* **372,** 421–424 (1994).
3. Bond, G. & Lotti, R. Iceberg discharge into the North Atlantic on millennial time scales during the last glaciation. *Science* **267,** 1005–1010 (1995).
4. Broecker, W. S., Bond, G., Klas, M., Bonani, G. & Wolfi, W. A salt oscillator in the glacial Atlantic? 1. The concept. *Paleoceanography* **5,** 469–477 (1990).
5. Lehman, S. J. & Keigwin, L. D. Sudden changes in North Atlantic circulation during the last deglaciation. *Nature* **356,** 757–762 (1992).
6. Behl, R. J. & Kennett, J. P. Brief interstandial events in the Santa Barbara basin, NE Pacific, during the past 60 kyr. *Nature* **379,** 243–246 (1996).
7. Oppo, D. W. & Lehman, S. J. Suborbital timescale variability of North Atlantic Deep Water during the past 200,000 years. *Paleoceanography* **10,** 901–910 (1995).
8. Oppo, D. W., McManus, J. F. & Cullen, J. C. Abrupt climate change events 500,000 to 340,000 years ago: evidence from subpolar North Atlantic sediments. *Science* **279,** 1335–1338 (1998).
9. Rasmussen, T. L., Thomsen, E., Labeyrie, L. & van Weering, T. C. E. Circulation changes in the Faeroe-Scotland Channel correlating with cold events during the last glacial period (58-10 ka). *Geology* **24,** 937–940 (1996).
10. MacAyeal, D. R. Binge/purge oscillations of the Laurentide ice sheet as a cause of the North Atlantic Heinrich events. *Paleoceanography* **8,** 775–784 (1993).
11. Rahmstorf, S. Rapid climate transitions in a coupled ocean–atmosphere model. *Nature* **372,** 82–85 (1994).
12. Suess, H. E. & Linick, T. W. The ^{14}C record in bristlecone pine of the past 8000 years based on the dendrochronology of the late C. W. Ferguson. *Phil. Trans. R. Soc. Lond. A* **330,** 403–412 (1990).
13. Pestiaux, P., van der Mersch, I., Berger, A. & Duplessy, J. C. Paleoclimatic variabiity at frequencies ranging from 1/10000 to 1/1000 years; evidence for nonlinear behaviour in the climate system. *Clim. Change* **12,** 9–37 (1988).
14. Yiou, P. *et al.* High frequency paleovariability in climate and CO_2 levels from the Vostok ice core records. *J. Geophys. Res.* **96,** 20365–20378 (1991).
15. Raymo, M. E. in *Start of a Glacial, Proc. Mallorca NATO ARW* 207–223 (eds Kukla, G. & Went, E.) (NATO ASI Ser. I, Vol. 3, Springer, Heidelberg, 1992).
16. Van Der Burgh, J., Visscher, H., Dilcher, D. L. & Kurschner, W. Paleoatmospheric signatures in Neogene fossil leaves. *Science* **260,** 1788–1790 (1993).
17. Raymo, M., Grant, B., Horowitz, M. & Rau, G. Mid-Pliocene warmth: stronger greenhouse and stronger conveyor. *Mar. Micropaleontol.* **27,** 313–326 (1996).
18. Kukla, G. & An, Z. Loess stratigraphy in central China. *Palaeogeogr. Palaeoclimatol. Palaeoecol.* **72,** 203–225 (1989).
19. Hooghiemstra, H. Quaternary and upper-Pliocene glaciations and forest development in the tropical Andes: evidence from a long high-resolution pollen record from the sedimentary basin of Bogata, Colombia. *Palaeogeogr. Palaeoclimatol. Palaeoecol.* **72,** 11–26 (1989).
20. Ruddiman, W. F., Raymo, M. E., Martinson, D. G., Clement, B. M. & Backman, J. Mid-Pleistocene evolution of Northern Hemisphere climate. *Paleoceanography* **4,** 353–412 (1989).
21. Wold, C. Cenozoic sediment accumulation on drifts in the northern North Atlantic. *Paleoceanography* **9,** 917–941 (1994).
22. Shipboard Scientific Party *Proc. ODP Init. Rep. Leg* **162,** 139–167 (1996).
23. Shackleton, N. J., Berger, A. & Peltier, W. R. An alternative astronomical calibration of the lower Pleistocene timescale based on ODP site 677. *Trans. R. Soc. Edinb. Earth Sci.* **81,** 251–261 (1990).
24. Channell, J. E. T., Hodell, D. & Lehman, B. Relative geomagnetic paleointensity and $\delta^{18}O$ at ODP Site 983 (Gardar Drift, North Atlantic) since 350 ka. *Earth Planet. Sci. Lett.* (submitted).
25. Ruddiman, W. F., Shackleton, N. J. & McIntyre, A. in *North Atlantic Palaeoceanography* (eds Summerhayes, C. P. & Shackleton, N. J.) 155–173 (Spec. Publ. 21, Geol. Soc., London, 1986).
26. Veum, T., Jansen, E., Arnold, M., Beyer, I. & Duplessy, J. C. Water mass exchange between the North Atlantic and the Norwegian Sea during the past 28,000 years. *Nature* **356,** 783–785 (1992).
27. Jansen, E. & Veum, T. Evidence for two-step deglaciation and its impact on North Atlantic deep-water circulation. *Nature* **343,** 612–616 (1990).
28. Lehman, S. J., Wright, D. G. & Stocker, T. F. in *Ice in the Climate System* (ed. Peltier, W. R.) 187–209 (NATO ASI Ser. I, Vol. 12, Springer-Verlag, Berlin, 1993).
29. Oppo, D. W. & Lehman, S. J. Mid-depth circulation of the subpolar North Atlantic during the last glacial maximum. *Science* **259,** 1148–1152 (1993).
30. Raymo, M. E. The timing of major climate terminations. *Paleoceanography* **12,** 577–585 (1997).
31. Wei, W. Calibration of upper Pliocene–lower Pleistocene nannofossil events with oxygen isotope stratigraphy. *Paleoceanography* **8,** 85–100 (1993).

Acknowledgements. We thank C. Rosario-Reyes and V. Vieira for assistance, and the Leg 162 Shipboard Scientific Party and crew for their accomplishments and dedication which made the collection of these cores possible. We also thank J. Adkins and T. Dokken for discussions which improved the manuscript. Samples were provided by the ODP with the support of the NSF.

Correspondence and requests for materials should be addressed to M.E.R. (e-mail: raymo@mit.edu).

Iron partitioning in a pyrolite mantle and the nature of the 410-km seismic discontinuity

Tetsuo Irifune & Maiko Isshiki

Department of Earth Sciences, Ehime University, Matsuyama 790, Japan

Pyrolite[1] is a hypothetical mixture of distinct minerals which is widely believed to represent the composition of the Earth's mantle. The main pressure-induced phase transformations of the olivine component of pyrolite occur at about 13.5 GPa (α to β) and 24 GPa (γ to $MgSiO_3$-rich perovskite + magnesiowüstite)[2,3], which are thought to be responsible for the seismic discontinuities at 410 and 660 km depths in the mantle. Recent seismological studies, however, have demonstrated that the 410-km seismic discontinuity is sharper in some areas than that expected from the α to β transformation in mantle olivine with a fixed composition[4–7]. Moreover, some mineral physics studies suggest that the seismic velocity jump at the 410-km discontinuity is inconsistent with that associated with the α to β transformation in olivine[8,9]. Here we present a phase equilibria study of a material having pyrolite composition at pressures of 6–16 GPa. We found that the iron content in olivine changes significantly with increasing pressure, as a result of the formation of a relatively iron-rich majorite phase at these pressures. This variation in iron content can overcome, or at least reduce, both of the above difficulties encountered with the pyrolite model of mantle composition, by showing that the component mineral systems cannot be treated as separate.

The pyrolite starting material was a powder of sintered oxide mixture, possessing an Mg number (Mg# = 100 Mg/(Mg + Fe)) of 89.0, which was used in our earlier study[10] at 23–28 GPa. A 4:6 mixture of "pyrolite minus olivine" glass[11] and natural olivine of formula $(Mg_{0.89}Fe_{0.11})_2SiO_4$ was also used in a few runs to check the equilibrium of the phases. The starting material was sealed in an $Au_{75}Pd_{25}$ capsule to prevent iron loss from the sample. The capsule was embedded in a platinum tube heater with a boron nitride insulator, and the temperature was monitored at the end of the capsule using a $W_{97}Re_3$–$W_{75}Re_{25}$ thermocouple without corrections for the effect of pressure on e.m.f. The temperature uncertainty may be of the order of ±50 °C, mainly due to a thermal gradient within the heater.

High-pressure runs were conducted using a multi-anvil system operated in a 2,000-ton press (ORANGE-2000) at Ehime University. The second-stage cube anvils were truncated by 5 mm edge length on the corners (truncation edge length (TEL) = 5.0), and semi-sintered magnesia was used as a pressure medium. Pressure was carefully calibrated against press load using phase transformations in some reference materials at both room temperature (I–II and III–V in Bi, semiconductor–metal in ZnS and GaAs) and high temperature (coesite–stishovite in SiO_2; olivine (α)–modified spinel (β) in Mg_2SiO_4), but may suffer uncertainties of the order of 0.2 GPa. Pressure was applied first, and then temperature was increased to the target value. Heating at the target temperature was conducted for several hours, and then the run was quenched. The recovered sample was examined by an electron microprobe and a micro-focus X-ray powder diffractometer.

Experimental conditions and results of the present runs are summarized in Table 1 and Fig. 1. Runs were conducted at 6–16 GPa at temperatures along a representative geotherm[12]. Electron-microprobe analyses using a broad electron beam demonstrated that there was virtually no iron loss throughout the charge in all of these runs. The α and β phases of olivine crystallized to give